Journal of Materials Chemistry A

ROYAL SOCIETY OF CHEMISTRY

PAPER

View Article Online
View Journal | View Issue

Cite this: J. Mater. Chem. A, 2026, 14, 9530

Highly conductive ester-based solid electrolyte exhibiting remarkable stability for safe, sustainable, and high-performance lithium metal batteries

Yunfan Shao, [a] Wanlin Chen [b] and Cristina Iojoiu *[ac]

Since the 1970s, polymer electrolytes (PEs) such as poly(ethylene oxide) (PEO) have been extensively studied to address the instability and safety issues associated with lithium metal electrodes. However, these conventional PEs suffer from low lithium transference numbers and narrow electrochemical stability windows. In this work, we introduce innovative solid-state PEs based on crosslinked poly(butyl malonate) (CPBM) and lithium salts. Unlike traditional PEO-based PEs, CPBM-based PEs are fully amorphous and self-standing, offering a suite of superior electrochemical properties. Notably, they exhibit comparable ionic conductivities to PEO-based PEs but achieve significantly higher lithium transference numbers and an impressive limiting current density enabling efficient ion transport. Another remarkable feature of our CPBM-based PEs is their wide electrochemical stability window, extending up to 4.7 V *vs.* Li/Li$^+$, and an excellent stability with lithium metal. These substantial improvements in electrochemical stability have been rigorously validated through long-term cycling stability tests, including Li stripping/plating and full cells with $LiFePO_4$ (LFP) and Mn-rich $LiMn_{0.6}Fe_{0.4}PO_4$ (LMFP) electrodes. We firmly believe that polymalonate-based PEs represent a pioneering solution to overcome the limitations inherent in PEO-based PEs and pave a way to safe, high-performance lithium metal batteries, marking a significant leap forward in battery technology.

Received 1st November 2025
Accepted 8th January 2026

DOI: 10.1039/d5ta08874g

rsc.li/materials-a

Introduction

Lithium-metal batteries (LMBs) and post-lithium batteries are highly anticipated as alternatives to traditional lithium-ion batteries with graphite negative electrodes.[1] Lithium metal, with its high specific capacity of 3860 mAh g^{-1} and low redox potential of −3.04 V *vs.* SHE, shows great promise as a next-generation negative electrode.[2] However, safety concerns, such as chemical and electrochemical instability, flammability,[3] dendrite formation,[4–6] and inhomogeneous solid electrolyte interphase (SEI) formation,[7,8] hinder its use with conventional organic liquid electrolytes, typically small molecule carbonates and ethers.[9]

To address the safety issues, polymer electrolytes (PEs) offer a promising alternative to flammable and volatile liquid electrolytes.[10,11] Various polymers, including polyethers,[12,13] polycarbonates,[14] fluoropolymers,[15] *etc.* have been investigated with different lithium salts. Among these, only very few provide good ionic conductivity under solvent/plasticizer-free conditions, known as "dry" polymer electrolytes.[16] Polyethers, particularly poly(ethylene oxide) (PEO)-based materials, are the most significant PEs for lithium ion batteries due to their ability to solubilize lithium salts and their flexible structures, which ensure high ionic conductivity in the amorphous phase.[17] However, PEO-based PEs face critical challenges when applied to high energy positive electrodes and lithium metal electrodes. They suffer from the oxidation of the ether bond at ~4 V *vs.* Li$^+$/Li which does not meet the voltage window of high energy positive electrodes such as lithium nickel manganese cobalt oxide (NMC), lithium nickel cobalt aluminum oxide (NCA), and lithium nickel manganese oxide (LNMO), whose redox potential exceeds 4.3 V *vs.* Li$^+$/Li.[18,19] Additionally, PEO-based PEs exhibit a low lithium transference number (T_{Li^+}, usually less than 0.2) due to the strong interaction between the ether oxygen atom and lithium cations leading to concentration gradients, extra polarization, limited critical current density and lithium dendrite formation.[20] Therefore, PEs with a broader electrochemical stability window (ESW) and higher T_{Li^+} could be promising candidates for next-generation PEs, targeting ether-free structures.

Aliphatic polycarbonates with a high dielectric constant such as poly(trimethylene carbonate) (PTMC)[14,21] and poly(propylene carbonate) (PPC)[22,23] have shown good ionic conductivity and T_{Li^+}. However, polycarbonate-based PEs suffer from chemical instability, *i.e.*, depolymerization, when used with Li-metal

[a]Univ. Grenoble Alpes, Univ. Savoie Mont Blanc, CNRS, Grenoble INP, LEPMI, 38000 Grenoble, France. E-mail: Cristina.Iojoiu@grenoble-inp.fr
[b]Department of Physical Chemistry II, Ruhr-Universität Bochum, 44801 Bochum, Germany
[c]Réseau sur le Stockage Electrochimique de l'Energie (RS2E), CNRS, FR3459, 80039 Amiens Cedex, France

electrodes.[24] Polyesters like polycaprolactone (PCL),[25,26] poly(-pentanediol adipate) (PEA),[27] poly(hexamethylene succinate) (PHS),[28,29] fluorinated polyesters[30] and ester-containing polymers[31] have been studied recently, exhibiting promising ionic conductivity and potential advantages in recycling. As predicted by molecular dynamic models of Chen *et al.*,[32] ester-containing polymers like PCL and poly(methyl methacrylate) (PMMA) have a low valence band minimum or high oxidation potential, suggesting a better stability at high voltages (>4 V *vs.* Li^+/Li) compared to polyethers. However, the stability of polyesters in the presence of lithium remains a concern. The highly reductive and basic environment near the lithium metal surface can lead to the degradation of the ester functionality, resulting in the formation of an unpredictable SEI layer.[33,34] A very recent study by Yang *et al.*[35] has shed light on the degradation mechanism of the ester function on the Li metal electrode due to the Claisen ester condensation reaction. This reaction is catalyzed by strong bases such as Li^0 or alkoxides, potentially affecting the ester molecules including PCL and PEA.

Among the various polyesters, polymalonates show unique potential in preventing the Claisen condensation reaction and may exhibit better stability compared to other polyesters. These polymers were first introduced in PEs in the early 2000s by Lee *et al.*[36] Balsara and coworkers[37–39] recently reported PEs based on poly(pentyl malonate)/LiTFSI which showed an amorphous structure and feasible ion transportation. More importantly, polymalonate-based PEs present a promising avenue for enhancing ion conduction and addressing the voltage constraints of traditional poly(ethylene oxide) (PEO)-based PEs in high-performance lithium metal batteries. However, the reported polymalonates are viscous liquids and lack mechanical strength, hindering their application in solid-state batteries. Furthermore, none of these studies demonstrated the cycling performance of polymalonate-based electrolytes in full cells with a positive electrode, leaving their performance as PEs unconfirmed.

This study introduces for the first time innovative SPEs based on crosslinked poly(butyl malonate) (CPBM) and evaluates their performance with two different lithium salts: lithium bis(trifluoromethanesulfonyl) imide (LiTFSI) and lithium bis(fluorosulfonyl) imide (LiFSI). The polymalonate polymers undergo crosslinking through a Michael addition reaction[40] (Scheme S1) with divinyl sulfone under basic conditions, resulting in a 3D network with adjustable crosslinking degrees. The resulting CPBM-based electrolytes are thermoset, meaning that they do not melt or dissolve, thus qualifying as true SPEs. These electrolytes offer unprecedented advantages in cost-efficiency, sustainability, and electrochemical performance, positioning them as a superior alternative to conventional PEO-based SPEs. In this work we addressed several critical questions and we demonstrated (i) the feasibility of developing a genuine SPE using polymalonate, (ii) that the ester functions of this SPE maintain excellent stability when paired with metallic lithium electrodes, and (iii) that the polymalonate-based PEs are compatible with high-voltage positive electrodes.

Results and discussion

SPE preparation

The synthesis of PBM was carried out through a transesterification reaction as illustrated in Fig. 1a. The structure of the polymalonate was confirmed by the ^1H and ^{13}C NMR spectra which are shown in Fig. S1 and S2. The resulting polymer has a number averaged molecular weight of 12 kg mol^{-1} and a polydispersity index of 1.8 as measured by size exclusion chromatography (SEC, Table S1). Due to the highly activated hydrogen from the methylene between the two carbonyl moieties, PBM can undergo crosslinking *via* a rapid Michael addition reaction. This process forms a solid-state, self-standing thermoset membrane, named CPBM (Fig. 1b). The images of the PBM and CPBM polymers are shown in Fig. S3. To balance mechanical strength while maintaining high chain flexibility, a relatively low amount of crosslinker is introduced, resulting in a molecular weight between crosslinks (M_c) of approximately 2 kg mol^{-1} in the final CPBM. The ATR-FTIR spectra of PBM and CPBM are shown in Fig. S4, displaying nearly identical vibration bands (except a tiny bump from S=O bond stretching at 1310 cm^{-1}).

The SPEs incorporating LiTFSI and LiFSI salts were prepared by directly dissolving the salt in the polymer followed by

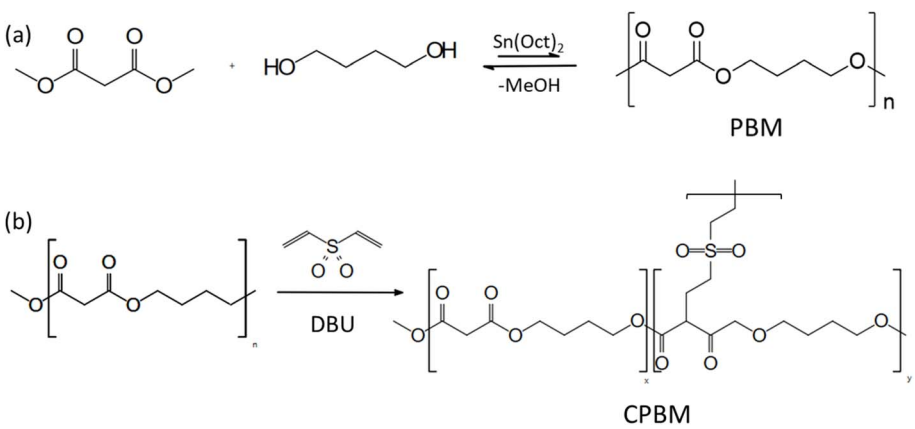

Fig. 1 (a) Synthesis route of the PBM polymer. (b) Chemical crosslinking of the CPBM polymer.

crosslinking. These are referred to as CPBM/LiTFSI and CPBM/LiFSI, respectively.

Thermal stability

Thermal stability of the PBM, CPBM, CPBM/LiTFSI and CPBM/LiFSI PEs was assessed by thermogravimetric analysis (TGA), with the thermograms presented in Fig. 2a. All the samples exhibited decomposition temperatures (1 wt%) exceeding 220 °C, indicating satisfactory thermal stability. Both PBM and CPBM polymers demonstrated identical thermal decomposition behavior, characterized by depolymerization of the polyester at around 350 °C. However, the addition of lithium salts lowered the decomposition temperature, likely due to the catalytic effect of the salts—especially in the case of LiTFSI.[41] Notably, the CPBM/LiFSI sample decomposed at ~230 °C, which can be attributed to the degradation of the LiFSI salt.[42] For comparison, the thermal degradation curves of PEO/LiFSI and PEO/LiTFSI (O/Li = 28) are included in Fig. S5. The degradation occurs at higher temperatures compared to CPBM electrolytes, and the presence of LiTFSI does not significantly affect the polymer stability (degradation temperature 400 °C).[43] Given the transesterification reaction, used to synthesize the polymalonate, which is a reversible reaction, the depolymerization through an alcoholysis reaction can revert the polymer back to its monomers. This process enables a closed-loop recycling of the polymer electrolyte[44] highlighting excellent sustainability prospects for these ester-based polymer electrolytes.

Ion transport

Lithium-ion conduction in SPEs is highly dependent on polymer chain mobility (reflected by glass transition temperature T_g) owing to the "hopping" mechanism in the amorphous phase. The T_g of the polymers and SPEs was evaluated by differential scanning calorimetry (DSC), with the DSC thermogram shown in Fig. 2b. PBM, CPBM, CPBM/LiTFSI and CPBM/LiFSI exhibited fully amorphous structures with no crystallization or melting peaks. The T_g values were observed at −52, −49, −24, and −18 °C, respectively. The amorphous structure and low T_g indicate an excellent chain flexibility of PBM, which is advantageous for fast ion transport.

The ionic conductivities of the CPBM/LiTFSI and CPBM/LiFSI SPEs are shown in Fig. 2c. Both electrolytes were prepared with the same O/Li ratio of 28. The ionic conductivity–temperature relationship followed a typical VTF type trend, indicating that the ion conduction was dominated by polymer chain motion[45] (Fig. S6 and Table S2). The CPBM/LiTFSI SPE demonstrated higher ionic conductivity compared to CPBM/LiFSI SPE, which is consistent with their T_g. At 80 °C, the two SPEs exhibited an ionic conductivity of 1.5×10^{-4} and 9.1×10^{-5} S cm^{-1} respectively.

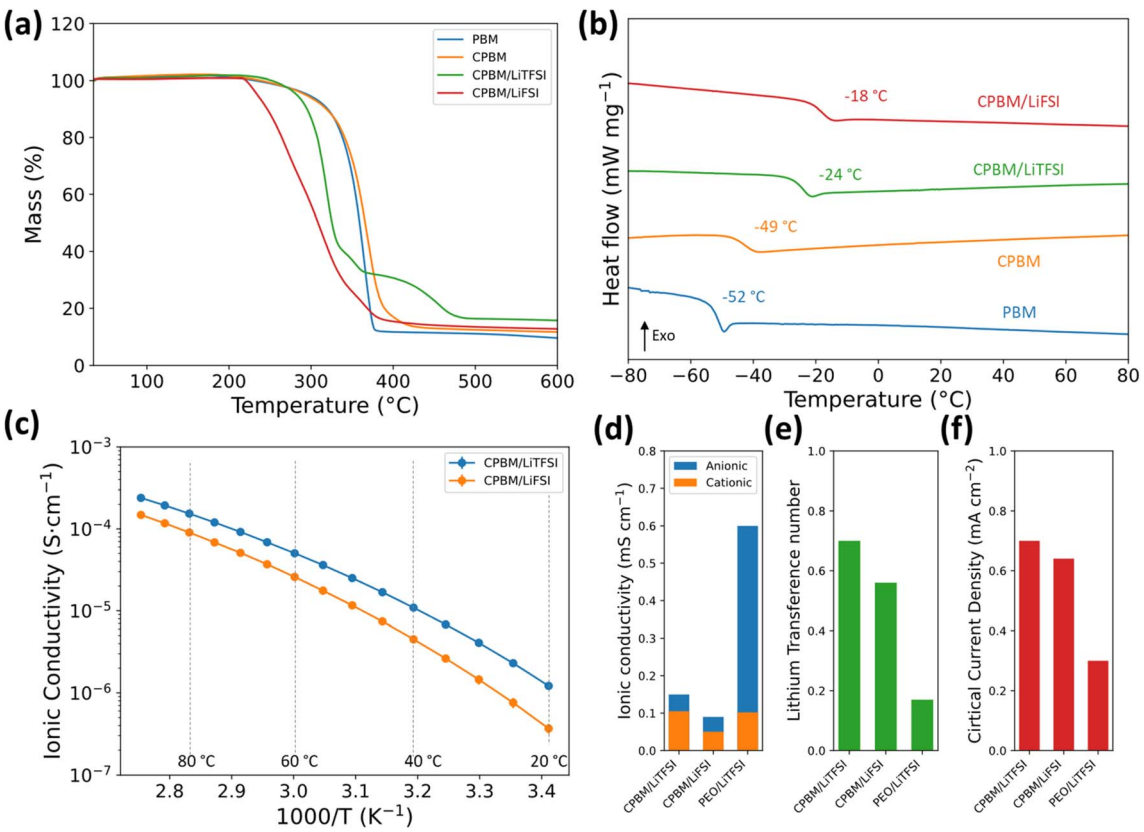

Fig. 2 (a) Thermogram of the PBM polymers and SPEs. (b) DSC traces of the PBM polymers and SPEs. (c) Ionic conductivity of the SPEs as a function of temperature. (d–f) Comparison between CPBM–LiTFSI, CPBM–LiFSI and PEO–LiTFSI SPEs at 80 °C in ionic conductivity, lithium transference number and critical current density, respectively. The data of PEO/LiTFSI were adopted from ref. 46, 48 and 50.

In addition to ionic conductivity, the lithium transference number (T_{Li^+}) is the other crucial parameter for evaluating the ion transport capability of the electrolytes. The T_{Li^+} of the CPBM–LiTFSI and CPBM–LiFSI SPEs were measured using electrochemical methods including a modified Bruce–Vincent method and Watanabe method, yielding lithium transference numbers of 0.70 and 0.55 respectively (Fig. S7 and S8). These ester-based SPEs exhibited much higher T_{Li^+}, up to three times higher, compared to the PEO-based polymer electrolytes, which generally have T_{Li^+} values around 0.15.[46] This significant improvement is due to the weaker interaction between the carbonyl functions and the Li^+ cation. As noted by Diederichsen *et al.*,[47] the higher T_{Li^+} can effectively reduce the cell polarization and enhance performance at high-power. The cationic conductivity of the SPEs can be calculated by multiplying the ionic conductivity with the lithium transference number: $\sigma_{Li^+} = \sigma \times T_{Li^+}$, reflecting their actual capability of Li^+ ion transportation. The CPBM-based SPEs exhibited cationic conductivity comparable with that of PEO/LiTFSI, which is around 0.1 mS cm^{-1} at 80 °C.[46]

Critical current density (CCD) of CPBM/LiTFSI and CPBM/LiFSI SPEs was evaluated by current scan experiments with symmetric Li|SPE|Li cells (Fig. S9 and S10). At low current density, the cell voltage–current density evolution followed Ohm's law, showing a linear correlation corresponding to a constant first order deviation (dE/dj). As the current density approached the critical value, additional polarization occurred, due to insufficient Li^+ diffusion, leading to depletion of Li^+ at the surface of the working electrode.[48,49] For CPBM/LiTFSI and CPBM/LiFSI, CCDs are determined to be 0.70 and 0.55 mA cm^{-2} respectively, which are significantly higher than that of PEO-based electrolytes, which is typically ~0.3 mA cm^{-2}.[50,51] Notably, the cell voltage transitions in CPBM-based SPEs were very sharp and dramatic, indicating a strict limit for the applied current density. This behavior is very different from that of the other examined PEs using a similar method, where the transition is usually mild and gradual.

The summary of ion transport behaviors, as depicted in Fig. 2d–f, compares the performance of CPBM-based solid polymer electrolytes (SPEs) with that of the widely used PEO/LiTFSI system. The comparison reveals that CPBM-based SPEs exhibit comparable or superior performance in various aspects of ion transport, particularly in the transference number and CCD. Additionally, lithium diffusion is more effectively promoted in the CPBM/LiTFSI system compared to CPBM/LiFSI. This suggests that CPBM-based SPEs, especially when paired with LiTFSI, offer enhanced ion transport properties, making them a promising alternative to traditional PEO-based electrolytes.

Structural and energetic analysis

To gain deeper insights into differing behavior of two lithium salts and lithium diffusion, molecular dynamics (MD) simulations were performed on two lithium salts (LiTFSI and LiFSI) dissolved in PBM. The diffusion of lithium salts within polymer electrolytes is heavily influenced by the ability of lithium ions to escape their solvation shells.[52,53] This process is governed by an activation free energy, which represents the energy barrier required to disrupt the interactions between lithium ions (Li^+) and oxygen atoms in their solvation environment. This barrier is intricately connected to the structure of the solvation shell surrounding Li^+ cations. To explore this phenomenon, molecular dynamics (MD) simulations were conducted on two lithium salts (LiTFSI and LiFSI) dissolved in PBM polymers. The investigation started with the calculation of the radial distribution function $g(r)$ between Li^+ ions and oxygens belonging to both PBM chains and $TFSI^-$ or FSI^- anions. The results, illustrated in Fig. 3a and b, revealed that the first peak in the $g(r)$ curves, which corresponds to the first solvation shell, was narrower and more intense for both the anion and PBM in the case of FSI^- compared to $TFSI^-$. This suggests that the solvation shell is more structured for FSI^-.

To quantify the energy required for Li^+ ions to shed their solvation shell, the potential of mean force (PMF), $\Delta G(r)$, was calculated from radial distribution functions using the equation

$$\Delta G(r) = -k_B T \ln g(r)$$

where k_B is Boltzmann's constant and T is the temperature. The PMF curves, shown in Fig. 3c and d, featured a minimum at the first solvation shell indicating the most probable coordination distance, followed by a maximum that corresponds to the energy for lithium to escape the shell. The difference between the maximum and the minimum provides an estimate of the free energy barrier associated with dissolution. This free energy barrier is proportional to the activation energy E_a for Li^+ diffusion, assuming a solvation-limited diffusion mechanism:

$$D \propto \exp\left(-\frac{E_a}{k_B T}\right), \quad \text{with} \quad E_a \propto \Delta G_{barrier}$$

This study found that the activation energy for Li^+ diffusion is lower in the $TFSI^-$ system compared to the FSI^- system for both PBM and anion-coordinated cases. This suggests that Li^+ diffusion is facilitated by the less structured solvation shell in the presence of $TFSI^-$.

To further understand the origin of this difference, the number of PBM chains and anions contributing to the solvation shell (defined by the first minimum of $g(r)$) was quantified as a function of Li^+ salt concentration (n_O/n_{Li}). Fig. 3e and f show that $TFSI^-$ ions consistently exhibit a higher number of coordinating PBM chains than FSI^-, across all concentrations. This suggests a more flexible solvation environment that facilitates cation hopping and is fully aligned with all the experimental results on transport properties. Additionally, the involvement of more polymer chains may introduce a greater steric hindrance, which is consistent with the lower overall coordination observed in the Li–O $g(r)$ curves for $TFSI^-$ as indicated by the intensity of the first peak. This trend aligns with a recent study[37] that suggests that the participation of more polymer chains in the Li^+ solvation shell promotes cation hopping. Fig. 3g and h provides a snapshot and illustration of the solvation structures.

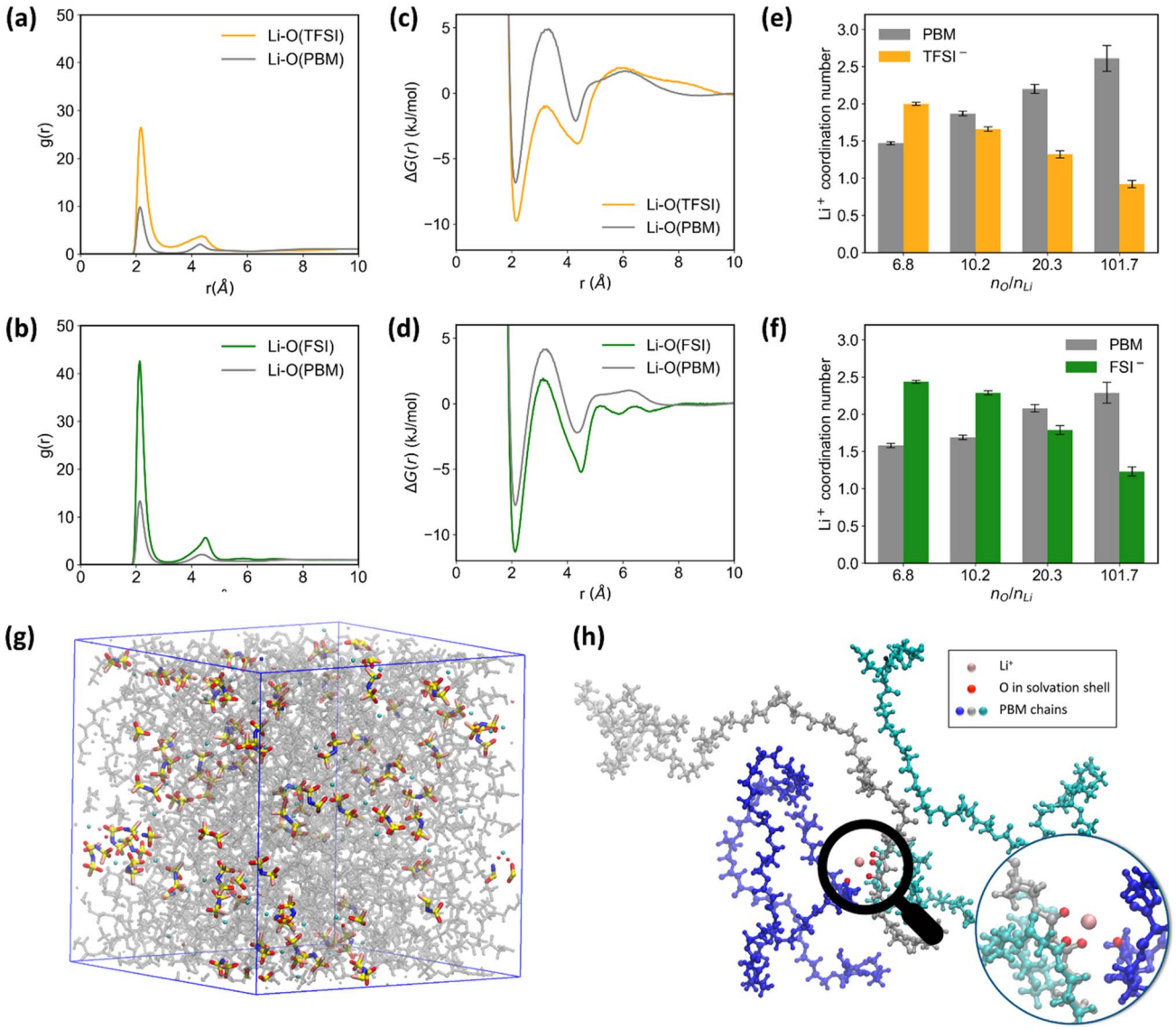

Fig. 3 Structural and energy analysis of Li^+ salt (LiTFSI/FSI) solvation in PBM polymers from MD simulations: radial distribution function $g(r)$ between Li^+ and oxygen atoms of (a) $TFSI^-$ and (b) FSI^- and PBM polymers. Potential of mean force of Li–O of (c) $TFSI^-$ and (d) $TFSI^-$ systems. The number of PBM chains in the solvation shell of Li^+ as a function of Li^+ salt concentration (n_O/n_{Li}) in the presence of (e) $TFSI^-$ and (f) FSI^-. (g) Snapshot of the MD simulation box of the PBM-based PE. (h) Schematic illustration of multiple PBM chains involved in the solvation shell of Li^+, providing a more flexible solvation environment, which facilitates cation hopping.

These findings emphasize the role of the solvation shell's composition and structure in determining ionic transport properties in polymer electrolytes, which is fully demonstrated by the experimental results.

The interaction between the lithium salt and polymer PBM was characterized by Raman spectroscopy (Fig. 4a). PBM/LiTFSI was prepared with varied O : Li ratios from 7 to 56. The S–N–S bending signal from $TFSI^-$ was observed between 725 and 775 cm^{-1}. With the increasing lithium concentration, the peak position was shifted from 740 (O : Li = 56) to 744 (O : Li = 7). This blue shift could be ascribed to the different supramolecular structure of the $TFSI^-$ anion; the 740 cm^{-1} band could represent the solvent separated ions (SSIs), and the 746 cm^{-1} band was due to the contact ion pairs (CIPs).[54,55] The CIP and SSI were deconvoluted and are presented in Fig. 4b. Notably, the aggregations of the LiTFSI salt (assigned to the bump at 760 cm^{-1}) remained at a very low ratio among all the different LiTFSI concentrations, reflecting a good dissociation of LiTFSI in the PBM polymer. Similar Raman spectra were collected with PBM/LiFSI samples (Fig. 4c). The S–N–S bending in the FSI^- anion could be assigned to the peak between 700 and 760 cm^{-1}. Blue shift of the peak was noticed with the FSI^-, which could be ascribed to the increasing CIP content with a higher LiFSI concentration, which follows a similar trend to that observed with LiTFSI.[56,57] With increasing concentration, the ratio between SSI and CIP decreased as depicted in Fig. 4d, which

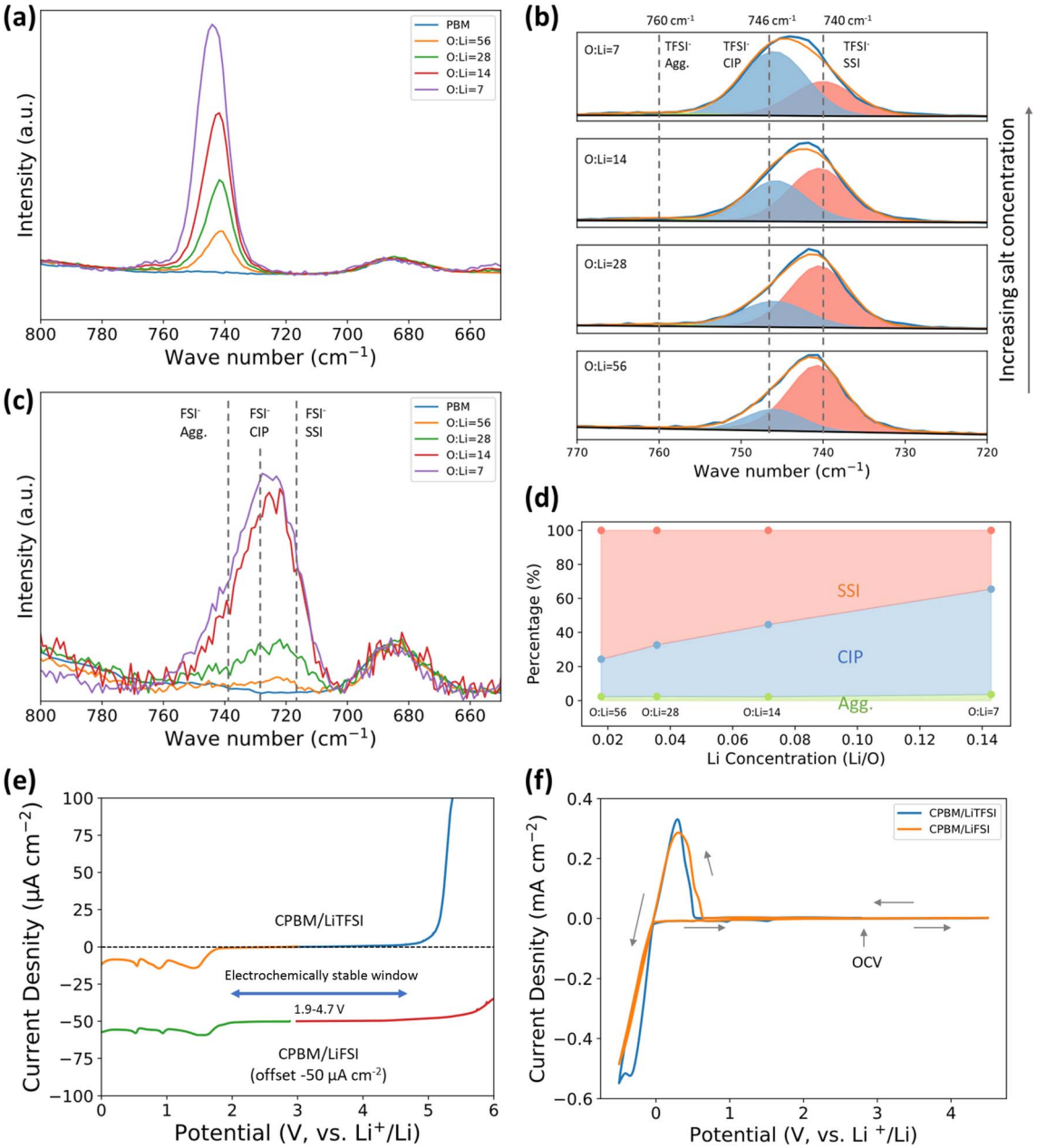

Fig. 4 (a) Raman spectra of PBM/LiTFSI mixtures in the region between 800 and 650 cm^{-1}. (b) Deconvolution of the spectra in (a). (c) Raman spectra of PBM/LiFSI mixtures in the region between 800 and 650 cm^{-1}. (d) The percentage of the three species as a function of lithium concentration. (e) Linear sweep voltammograms of Li|SPE|SS cells at 80 °C, with a sweep rate of 0.1 mV s^{-1}; the trace of CPBM–LiFSI is offset by −0.05 mA cm^{-2}. (f) Cyclic voltammograms of Li|SPE|SS cells at 80 °C, swept between −0.5 and 4.5 V *vs.* Li^+/Li with a sweep rate of 0.1 mV s^{-1}.

aligned with the results from the MD simulations. Optimal dissolution and dissociation of both LiTFSI and LiFSI could be realized in a wide range of salt concentrations, which ensures promising ion transport behaviors in PBM-based polymer electrolytes.

Electrochemical stability

The electrochemical stability window of the SPEs is initially evaluated using linear sweep voltammetry with Li|SPE|SS cells at 80 °C, as shown in Fig. 4e. During the anodic scans, oxidation began at ~4.7 V. The electrolyte containing LiTFSI exhibited strong oxidation beyond this voltage, whereas CPBM/LiFSI showed much milder oxidation compared to LiTFSI. This could be attributed to a better passivation by the FSI^- group at the surface of the working electrode. In the cathodic scans, reduction peaks are observed between 0.5 and 1.9 V *vs.* Li^+/Li. These peaks are commonly seen in various polymer electrolytes, which are very likely related to the reduction of surface oxide on the working electrodes.[58] In summary, the CPBM polymer with both LiTFSI and LiFSI salts has a wide electrochemical stability window between 1.9 and 4.7 V *vs.* Li^+/Li.

To further examine this ESW, cyclic voltammetry was performed between −0.5 and 4.5 V *vs.* Li^+/Li (Fig. 4f). As expected, no oxidation is observed up to 4.7 V and well-defined lithium plating and stripping occurred between −0.5 and 1 V *vs.* Li^+/Li.

Lithium stripping/plating

Lithium stripping/plating tests were conducted with symmetrical Li cells at different current densities to examine the compatibility between SPEs and the Li metal electrode. The voltage profiles of lithium stripping/plating tests at 80 °C are shown in Fig. 5a, b, S11 and S12 for both CPBM/LiFSI and CPBM/LiTFSI SPEs respectively. The tests were conducted with current densities of 50, 100, 200, 400, and 500 μA cm^{-2} and returned to 100 μA cm^{-2}, corresponding to capacities of 0.2, 0.4, 0.8, 1.6 and 2.0 mAh. Both cells showed stable and symmetrical overpotential during stripping/plating even at the highest current density at 500 μA cm^{-2}. For each half-cycle of 4 h, 2 mAh cm^{-2} of lithium is stripped/plated, corresponding to ~10 μm thickness of lithium metal. After the tests with varied current density, the cell with CPBM–LiFSI SPE was cycled at 100 μA

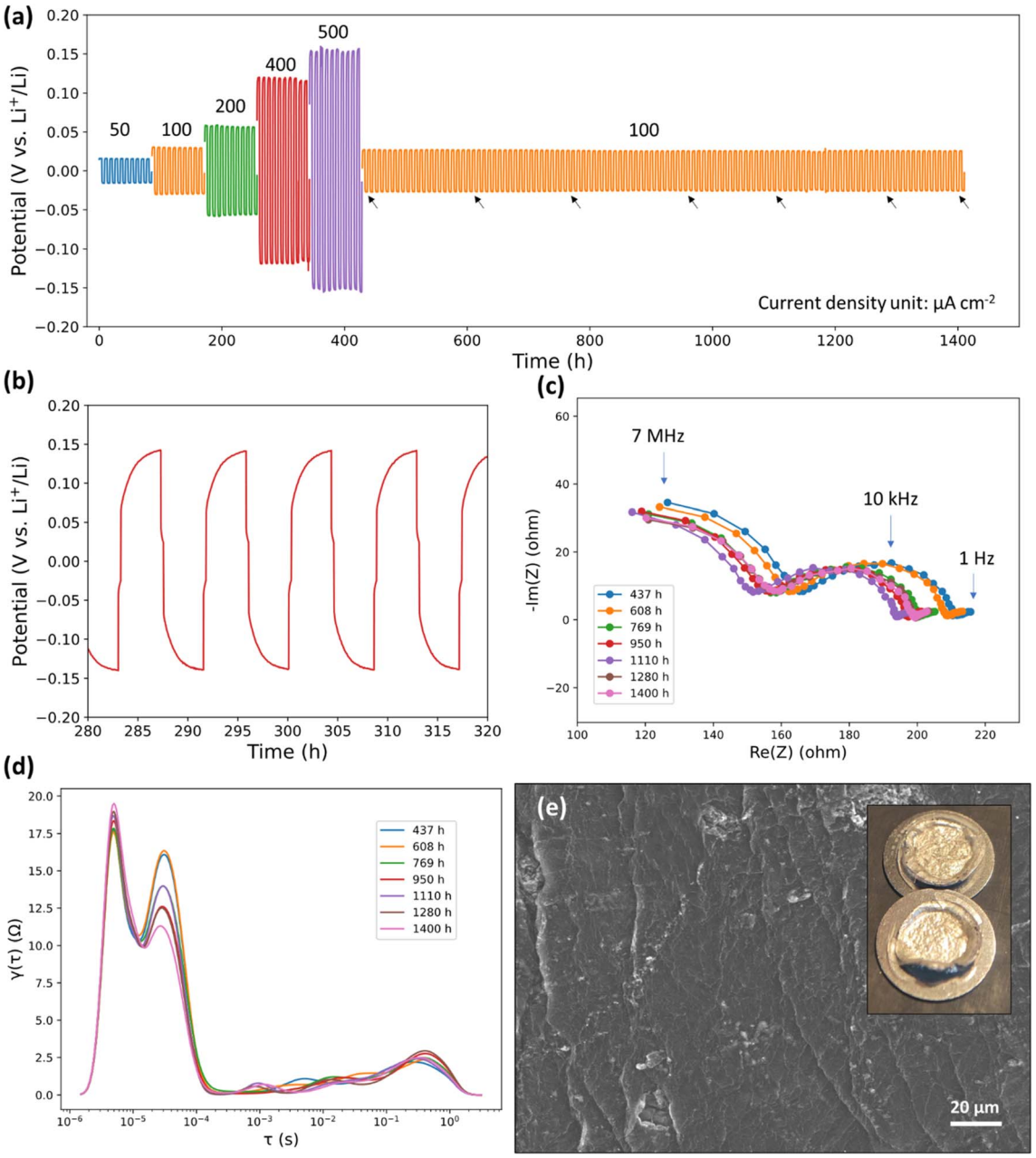

Fig. 5 (a) Lithium stripping/plating test at various current densities using Li|SPE|Li cells at 80 °C with CPBM–LiFSI SPE. The arrows indicate the selected EIS spectra. (b) Magnification of the potential profiles between 280 and 320 h, with a current density of 400 μA cm^{-2}. (c) Selected EIS spectra during the stripping/plating test. (d) DRT of the interfacial response of the Li|SPE|Li cells during the lithium plating/stripping. (e) SEM image of the lithium|SIPE interface after 1400 h of lithium stripping/plating tests. The inset shows images of the Li electrode after 1400 h of cycling.

cm^{-2} for around 1000 h. EIS spectra (Fig. 5c and S13) were recorded during the stripping/plating to follow the evolution of the Li|SPE interphases. The EIS spectra displayed a two-semicircle shape, corresponding to electrolyte bulk resistance at high frequency and interfacial resistance at middle frequency. A minor decrease in the bulk resistance was observed between 400 and 780 h and remained stable afterwards, which could be ascribed to establishment of the SEI. The interfacial resistance remained almost constant at around 40 Ω cm^{-2} during the experiments, reflecting excellent stability against lithium. To better deconvolute the interfacial responses, the EIS spectra at middle-low frequency (220 kHz to 1 Hz) were converted into distribution of relaxation times (DRT).[59] (Fig. 5d). The DRT showed two different relaxation times (5.2×10^{-6} and 3.1×10^{-5} s), while only one semicircle was observed on the Nyquist plot. The second relaxation time decreased with increasing cycling time, indicating an improved SEI evolution during lithium stripping/plating. An additional peak was observed between 10^{-1} to 10^{0} (10^{-1} Hz), which might reflect the charge transfer behavior.[60] Similarly, long-term stripping/plating tests were conducted with CPBM/LiTFSI cells, showing ideal stability and no evidence for lithium dendrite formation.

Ex situ SEM images of the lithium were obtained after disassembling the cells from Li stripping/plating experiments for both CPBM/LiFSI and CPBM/LiFSI (Fig. 5e and S14, respectively). After more than 1000 h of lithium stripping/plating experiments, the lithium metal electrodes retained the silver-white color and shining metallic luster. SEM images revealed a smooth surface of lithium without any mossy or dendritic species providing solid evidence for stable and dendrite-free lithium stripping/plating of CPBM-based SPEs.

These results demonstrated excellent stability of the SPEs against the lithium metal electrode, with no lithium dendrite formation.

In addition, asymmetric lithium stripping/plating with Li|SPE|Cu cells were performed to examine the lithium reversibility (Fig. S15). The experiment was carried out using a modified method adopted from Adams *et al.*[61] to determine the coulombic efficiency (CE). A preconditioning process of a long depletive plating/stripping cycle was applied to the Cu working electrode to rule out the influence of side reactions and surface oxides. After this preconditioning, 2 mAh cm^{-2} of Li was plated on the Cu as a reservoir, followed by lithium stripping/plating (0.1 mAh cm^{-2} per cycle) until the Li reservoir was fully depleted (indicated by an increase in the voltage). The final CE could be calculated from the ratio between the total amount of lithium stripped and total amount of lithium plated including the reservoir. This experiment lasted for 158 cycles until the lithium on Cu was fully consumed, which corresponds to an average CE of ~90%. The imperfection of the CE reflects the formation of electrochemically isolated lithium (so-called "dead" lithium), which is more significant when using solid-state electrolytes. The previously reported values are mostly around 85% in different polymers.[62,63] Thus, to the best of our knowledge, the CPBM-based SPEs showed the best lithium reversibility within the polymer electrolytes.

SEI formation mechanism

The ester function is usually considered unstable when in contact with the lithium metal electrode due to the strong basic and low redox potential condition near the lithium metal electrode. Depolymerization or a side reaction was observed in ester-based liquid electrolyte or polycarbonates.[24,34,64] Unexpectedly, the CPBM-based SPEs exhibited exceptional stability against lithium metal, maintaining stability over 1000 hours of cycling during lithium stripping/plating without interfacial degradation. To elucidate this behavior, it is essential to investigate the reaction between the polymer and lithium metal, focusing on the SEI formation mechanism and its composition.

Ex situ X-ray photoelectron spectroscopy (XPS) was used to analyze the polymer electrolyte and lithium metal before and after lithium stripping/plating experiments. On the polymer side, the F 1s, O 1s and C 1s spectra were examined, as shown in Fig. 6a, b and S16 for CPBM/LiFSI and CPBM/LiTFSI respectively. The CPBM SPEs, both pristine and after cycling, showed all expected moieties including hydrocarbon (C–C/C–H) at 285.0 eV and ester function at 286.3 eV (C–O) and 289.1 eV (O–C=O).[65,66] Fluorocarbon (C–F) at 292.1 eV was also observed in the presence of LiTFSI.[67] In O 1s spectra, ester function was found at 532.6 and 533.8 eV.[65] Importantly, the O 1s and C 1s spectra do not alter before and after cycling, suggesting a minimal degradation in the polymer matrix during the lithium stripping/plating process. Chemical information regarding the lithium salts is more apparent in F 1s spectra. Well-defined peaks of C–F from LiTFSI were observed at 689.0 eV, and the SO_2–F peak from the LiFSI salt was observed at ~688.0 eV. The degradation product LiF was found at 685.0 eV.[68] The overall intensity of the F 1s signal was decreased after cycling, suggesting that the F-containing species migrated to the surface of the lithium metal for SEI formation, especially in the case of more reactive LiFSI.

Simultaneously, the lithium metal was also examined by XPS after cycling (Fig. 6c, S17 and S18) to investigate the SEI formation. For both salts, inorganic compounds Li_2CO_3 (290.4 eV) and LiF (685.0 eV) and organic degradation products in C 1s (283.6 eV) and O 1s (528.8 eV) spectra were observed as the major compositions for the SEI layer. We suppose that the C 1s at 283.6 eV is related to the high reactivity of methyl malonate with lithium metal leading to different degradation products.[69] Minor degradation species from lithium salts such as Li_2S (160.9 eV), Li_3N (397.1 eV) are also detected.[67] The lithium carbonate likely originates from the native passivation layer on the lithium metal. The other inorganic species detected—LiF, Li_3N, and Li_2S—are products of lithium salt degradation. While LiF and Li_3N are typically favored SEI components due to their superior mechanical properties and effective passivation[70] the organic degradation products may play a more critical role in stabilization.[11,71] These organic species were only detected on the lithium surface, not on the polymer surface, indicating that degradation is localized to Li^0 and that the degraded layer is relatively thin (below the XPS detection limit of ~10 nm). We assume that polymer degradation occurs *via* a mechanism analogous to acyloin condensation, where Li^0 attacks the carbonyl moiety to generate radicals. Other potential

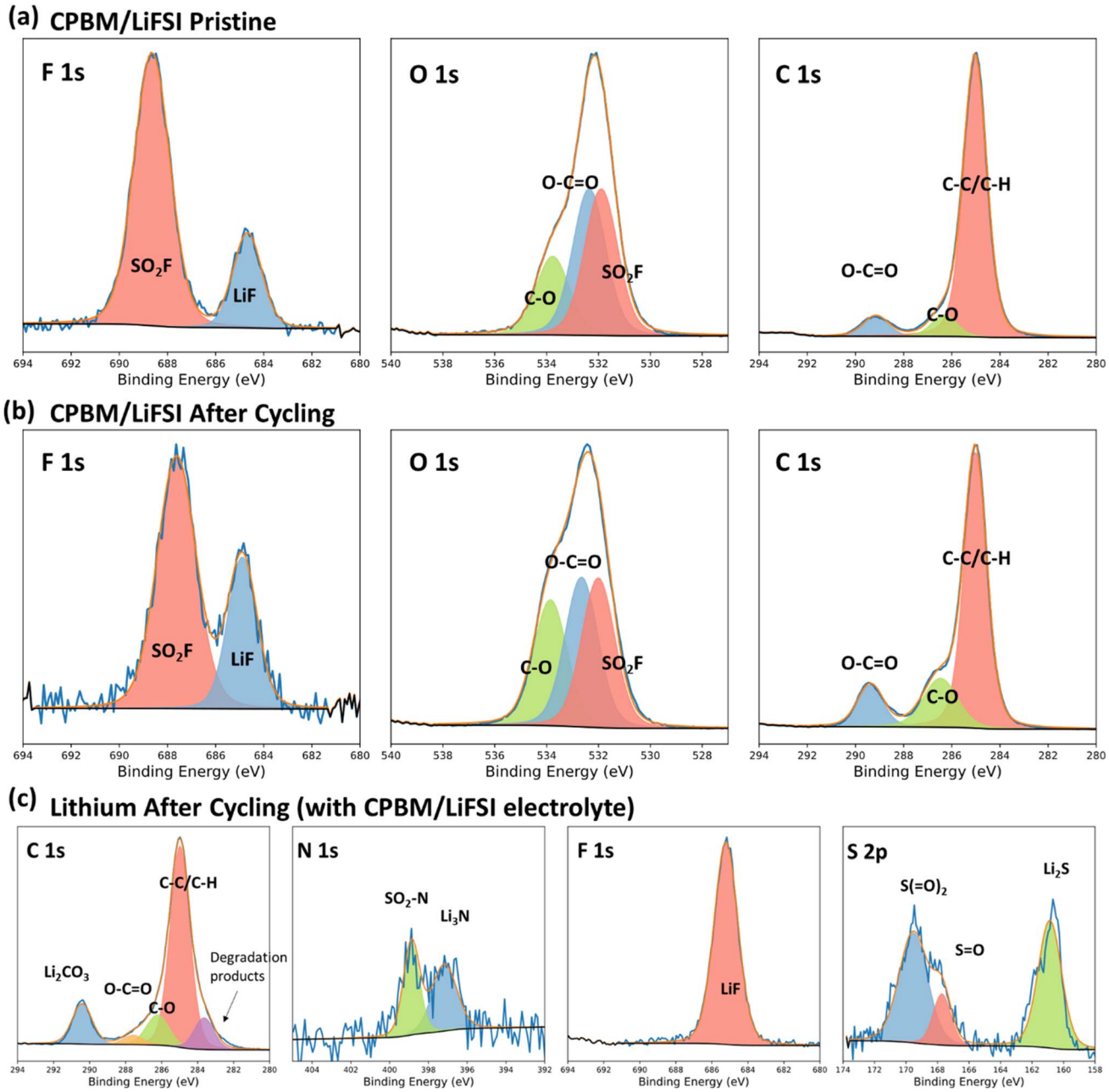

Fig. 6 Examination of SEI formation with XPS spectra: (a) pristine CPBM/LiFSI SPE membrane; (b) CPBM/LiFSI SPE after 50 h of lithium stripping/plating experiments; and (c) lithium surface after 50 h of lithium stripping/plating experiments.

degradation pathways, such as ester saponification or Claisen condensation, are unlikely under these conditions.[34] The degradation process is rapidly inhibited due to the passivation of the lithium surface. This inhibition is attributed to the synergistic effects of the solid-state electrolyte, which prevents surface renewal, and the passivation layer formed by salt degradation—particularly in the case of LiFSI. Together, these factors contribute to the formation of a thin yet robust SEI layer.

Evaluation in prototype LMBs

The CPBM-based SPEs were ultimately evaluated in LMB cells with $LiFePO_4$ (LFP) and Mn-rich $LiMn_{0.8}Fe_{0.2}PO_4$ (LMFP) positive electrodes at 80 °C. The specific capacity and CE of Li|SPE|LFP cells are shown in Fig. 7a, with corresponding discharge/charge profiles in Fig. S19 and S20. The cells underwent galvanostatic cycling at a C-rate of C/2 ($C = 170$ mA g^{-1}) for 500 cycles. An initial specific capacity of 158 mAh g^{-1} was found for both CPBM/LiTFSI and CPBM/LiFSI SPEs, reaching an almost full capacity for the LFP material. The specific capacity then slowly decayed to 112 and 127 mAh g^{-1} after 500 cycles, corresponding to a capacity retention of 71 and 80% respectively. Both SPEs exhibited nearly perfect capacity reversibly with an average CE of 99.8 and 99.9% for CPBM/LiTFSI and CPBM/LiFSI respectively. The CPBM/LiFSI SPE demonstrated

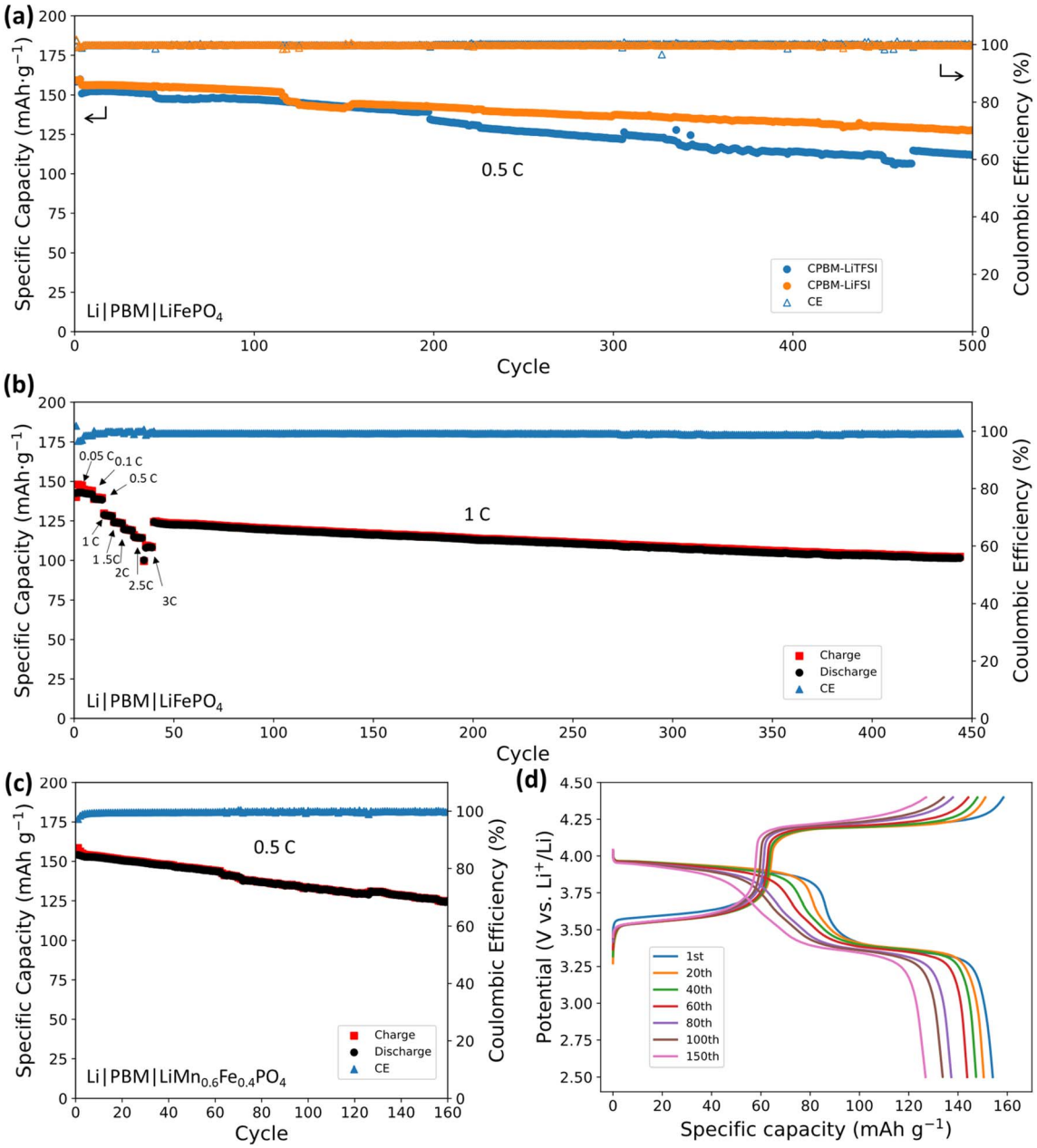

Fig. 7 (a) Long-term cycling test at a C-rate of 0.5C conducted on Li|SPE|LFP cells at 80 °C. (b) C-rate test and subsequent long-term cycling at 1C for Li|CPBM/LiTFSI|LFP cells at 80 °C. (c) Cycling test conducted on Li|CPBM/LiFSI|LMFP cells at 80 °C; (d) selected discharge/charge profiles for the LMFP cells.

overall better cycling stability compared to CPBM/LiTFSI SPE, exhibiting accordance with the results from lithium stripping/plating experiments.

The C-rate test of the Li|SPE|LFP cells was also conducted. For CPBM/LiTFSI SPE (Fig. 7b), the cell was cycled at 0.5, 1, 1.5, 2, 2.5 and 3C and then reduced to 1C for long cycling. Reversible capacities of 142, 138, 128, 123, 119, and 108 mAh g^{-1} were achieved from 0.5 to 3C respectively, outstanding results for a dry electrolyte. Compared to dry polymer electrolytes based on amorphous PEO, whether electrolytes based on a blend with LiTFSI[72,73] or single conducting polymer electrolyte,[16,17] the specific capacity of the CPBM/LiTFSI solid polymer electrolyte at 2C is more than twice as high. This result highlights the outstanding electrochemical performance of CPBM. The long cycling at 1C after the C-rate test lasted for another 400 cycles, with a capacity retention of 82%. For CPBM/LiFSI (Fig. S21), the maximum achievable C-rate was approximately 1C, yielding a capacity of only 84 mAh g^{-1}. These C-rate tests underscore the distinct advantage of LiTFSI salt over LiFSI under high power conditions, likely attributable to CPBM/LiFSI's higher ionic conductivity and greater T_{Li^+}.

Thanks to their straightforward processing, CPBM-based solid polymer electrolytes (SPEs) can be easily cast into large-scale thin films using doctor blading—a method highly

compatible with pouch cell fabrication. To demonstrate the potential for scaling up solid-state lithium metal batteries with CPBM-based SPEs, a single-layer prototype pouch cell (6.8 × 4.5 cm, Fig. S20) was successfully fabricated.

To assess performance across a broader electrochemical stability window, the LMFP positive electrode was paired with the CPBM/LiFSI solid polymer electrolyte. Li|SPE|LMFP cells were cycled between 2.5 V and 4.4 V (*vs.* Li^+/Li) for 160 cycles (Fig. 7c), achieving 84% capacity retention and an average coulombic efficiency (CE) of 99.7%. The charge/discharge profiles (Fig. 7d) revealed two distinct plateaus, corresponding to the redox reactions of Fe and Mn atoms. These results demonstrate the robust cycling stability of the cells and confirm the extended electrochemical stability of the malonate-based polymer electrolyte. Additionally, LMFP with a higher Mn content ($LiMn_{0.8}Fe_{0.2}PO_4$) was also cycled with CPBM/LiFSI. As shown in Fig. S23, the Mn-rich electrode retained 75% of its capacity and maintained an average CE of 99.3% over 70 cycles. However, achieving improved cycling stability with Mn-rich LMFP remains challenging due to issues such as CEI formation and Mn[74,75] which warrant further investigation.

In summary, the exceptional long-term cycling stability of Li|SPE|LFP cells strongly supports the viability of polymalonate-based solid polymer electrolytes (SPEs) for lithium metal batteries. Furthermore, their successful integration with high-voltage LMFP positive electrodes demonstrates the superior electrochemical stability of these polyesters compared to traditional polyethers.

Conclusions

In conclusion, this study successfully demonstrated the synthesis and application of poly(butyl malonate) as a novel solid polymer electrolyte for lithium metal batteries. Through a transesterification reaction and subsequent blending with lithium salts such as LiTFSI and LiFSI, we produced thin, flexible, and self-standing membranes *via* a casting process followed by crosslinking through a rapid Michael addition reaction. The resulting solid polymer electrolyte exhibited exceptional properties, including high ionic conductivity, transference number, critical current density, and electrochemical stability, surpassing the performance of current state-of-the-art polyether-based solid polymer electrolytes.

Notably, poly(butyl malonate) showed remarkable stability against lithium metal electrodes, with minimal degradation or short-circuiting observed over 1400 hours. This stability is attributed to the formation of a stable solid electrolyte interphase (SEI) between the polymer and lithium metal, as confirmed by X-ray photoelectron spectroscopy (XPS) characterization and extensive plating/stripping tests in both symmetrical and asymmetrical cells. The long-term cycling stability of Li|SPE|LFP cells underscores the potential of polymalonate-based solid polymer electrolytes in lithium metal batteries. Furthermore, the successful adaptation to LMFP positive electrodes with higher voltage highlights the extended electrochemical stability window of polyesters compared to polyethers.

The LiTFSI salt demonstrated superior ion transport behaviors, enhancing rate capability in cell performance, while LiFSI exhibited better electrochemical stability due to efficient passivation of the lithium metal electrode by a LiF-rich SEI. Overall, our findings suggest that poly(butyl malonate) is a promising and sustainable alternative to conventional polyester-based solid polymer electrolytes. Its potential depolymerization under mild conditions indicates a viable recycling route, further enhancing the sustainability of this low-cost polyester-based electrolyte. This research paves the way for the development of safe, sustainable, and high-performance lithium metal batteries.

Author contributions

C. I. and Y. S. conceived and designed the study. Y. S. performed the experiments and drafted the manuscript. W. C. contributed to the molecular dynamics modeling and analysis. The manuscript was written through contributions of all authors. All the authors discussed the results and commented on the manuscript.

Conflicts of interest

There are no conflicts to declare.

Data availability

Data for this article, including spectra and electrochemical measurements are available at Open Science Framework at https://doi.org/10.17605/OSF.IO/JSDAX.

Supplementary information (SI): experimental details and additional figures. The authors have cited additional references in the SI.[76–80] See DOI: https://doi.org/10.1039/d5ta08874g.

Acknowledgements

The authors would like to acknowledge the financial support from Carnot Institut Énergies du Futur. We would like to thank Mr Thomas Boulmier for SEM imaging, Mr Tony Bertaux for Raman measurements and Mr Vincent Martin for the XPS measurements. W. C. acknowledges the Alexander von Humboldt Foundation for a research fellowship under the Henriette-Hertz-Scouting Program and the RESOLV Cluster of Excellence (EXC 2033 – 390677874), funded by the Deutsche Forschungsgemeinschaft (German Research Foundation). This research has benefited from the characterization equipment of the Grenoble INP – CMTC platform supported by the Centre of Excellence of Multifunctional Architectured Materials ''CEMAM'' (grant ANR-10-LABX-44-01) funded by the ''Investments for the Future'' Program.

References

1 J. Asenbauer, T. Eisenmann, M. Kuenzel, A. Kazzazi, Z. Chen and D. Bresser, *Sustainable Energy Fuels*, 2020, **4**, 5387–5416.

2 D. Lin, Y. Liu and Y. Cui, *Nat. Nanotechnol.*, 2017, **12**, 194–206.
3 X. Feng, D. Ren, X. He and M. Ouyang, *Joule*, 2020, **4**, 743–770.
4 D. Cao, X. Sun, Q. Li, A. Natan, P. Xiang and H. Zhu, *Matter*, 2020, **3**, 57–94.
5 D. Stępień, B. Wolff, T. Diemant, G.-T. Kim, F. Hausen, D. Bresser and S. Passerini, *ACS Appl. Mater. Interfaces*, 2023, **15**, 25462–25472.
6 S. Menkin, J. B. Fritzke, R. Larner, C. De Leeuw, Y. Choi, A. B. Gunnarsdóttir and C. P. Grey, *Faraday Discuss.*, 2023, **248**, 277–297.
7 Q. Liu, A. Cresce, M. Schroeder, K. Xu, D. Mu, B. Wu, L. Shi and F. Wu, *Energy Storage Mater.*, 2019, **17**, 366–373.
8 E. K. W. Andersson, L.-T. Wu, L. Bertoli, Y.-C. Weng, D. Friesen, K. Elbouazzaoui, S. Bloch, R. Ovsyannikov, E. Giangrisostomi, D. Brandell, J. Mindemark, J.-C. Jiang and M. Hahlin, *J. Mater. Chem. A*, 2024, **12**, 9184–9199.
9 H. Wang, Z. Yu, X. Kong, S. C. Kim, D. T. Boyle, J. Qin, Z. Bao and Y. Cui, *Joule*, 2022, S2542435121005870.
10 J. Li, Y. Cai, H. Wu, Z. Yu, X. Yan, Q. Zhang, T. Z. Gao, K. Liu, X. Jia and Z. Bao, *Adv. Energy Mater.*, 2021, **11**, 2003239.
11 M. Li, S. Yang and B. Li, *Interdiscip. Mater.*, 2024, **3**, 805–834.
12 Z. Xue, D. He and X. Xie, *J. Mater. Chem. A*, 2015, **3**, 19218–19253.
13 D. G. Mackanic, W. Michaels, M. Lee, D. Feng, J. Lopez, J. Qin, Y. Cui and Z. Bao, *Adv. Energy Mater.*, 2018, **8**, 1800703.
14 B. Sun, J. Mindemark, K. Edström and D. Brandell, *Solid State Ionics*, 2014, **262**, 738–742.
15 T. K. L. Nguyen, G. Lopez, C. Iojoiu, R. Bouchet and B. Ameduri, *J. Power Sources*, 2021, **498**, 229920.
16 Y. Shao, F. Alloin, D. Bresser and C. Iojoiu, *J. Mater. Chem. A*, 2024, **12**, 30032–30040.
17 H. P. K. Ngo, Y. Shao, T. Bertaux, T. K. L. Nguyen, J. Solier, E. Planes, P. Judeinstein, F. Alloin, J.-Y. Sanchez and C. Iojoiu, *ACS Appl. Energy Mater.*, 2025, **8**, 2819–2827.
18 J. Kasnatscheew, B. Streipert, S. Röser, R. Wagner, I. Cekic Laskovic and M. Winter, *Phys. Chem. Chem. Phys.*, 2017, **19**, 16078–16086.
19 X. Yang, M. Jiang, X. Gao, D. Bao, Q. Sun, N. Holmes, H. Duan, S. Mukherjee, K. Adair, C. Zhao, J. Liang, W. Li, J. Li, Y. Liu, H. Huang, L. Zhang, S. Lu, Q. Lu, R. Li, C. V. Singh and X. Sun, *Energy Environ. Sci.*, 2020, **13**, 1318–1325.
20 S. Bublil, G. Peta, M. Fayena-Greenstein, H. Alon-Yehezkel, O. Raskin, Y. Elias and D. Aurbach, *J. Electrochem. Soc.*, 2022, **169**, 110523.
21 M. Ebadi, T. Eriksson, P. Mandal, L. T. Costa, C. M. Araujo, J. Mindemark and D. Brandell, *Macromolecules*, 2020, **53**, 764–774.
22 C. Wang, H. Zhang, J. Li, J. Chai, S. Dong and G. Cui, *J. Power Sources*, 2018, **397**, 157–161.
23 J. Zhang, J. Yang, T. Dong, M. Zhang, J. Chai, S. Dong, T. Wu, X. Zhou and G. Cui, *Small*, 2018, **14**, 1800821.
24 B. Commarieu, A. Paolella, S. Collin-Martin, C. Gagnon, A. Vijh, A. Guerfi and K. Zaghib, *J. Power Sources*, 2019, **436**, 226852.
25 J. Mindemark, E. Törmä, B. Sun and D. Brandell, *Polymer*, 2015, **63**, 91–98.
26 F. P. Nkosi, M. Valvo, J. Mindemark, N. A. Dzulkurnain, G. Hernández, A. Mahun, S. Abbrent, J. Brus, L. Kobera and K. Edström, *ACS Appl. Energy Mater.*, 2021, **4**, 2531–2542.
27 X. Xie, P. Zhang, X. Li, Z. Wang, X. Qin, M. Shao, L. Zhang and W. Zhou, *J. Am. Chem. Soc.*, 2024, **146**, 5940–5951.
28 Z. Yang, J. Cai, Z. Shen, J. Bian, J. Chen, Y. Xu, Z. Fang, C. Du, X. Xiang, J. Wang, P. Yu, R. Cui and S. Bi, *Macromolecules*, 2024, **57**, 4460–4470.
29 J. Chen, Q. Liu, Z. Shen, X. Peng, J. Bian, Z. Bao, Y. Chen and S. Bi, *Mater. Lett.*, 2025, **398**, 138882.
30 X. Dai, H. Ye, G. Huang and G. Li, *Adv. Mater.*, 2025, e11556.
31 Q. Zhang, T. Bian, X. Wang, R. Shi and Y. Zhao, *Angew. Chem.*, 2025, **137**, e202415343.
32 L. Chen, S. Venkatram, C. Kim, R. Batra, A. Chandrasekaran and R. Ramprasad, *Chem. Mater.*, 2019, **31**, 4598–4604.
33 D. Aurbach, *Solid State Ionics*, 2002, **148**, 405–416.
34 M. Grünebaum, A. Buchheit, C. Lürenbaum, M. Winter and H.-D. Wiemhöfer, *J. Phys. Chem. C*, 2019, **123**, 7033–7044.
35 Y. Yang, L. Yu, Y. Huang, X. Ding, Z. Xue, Z. Li, Y. Yao, S. Zhang, L. Xu, X. Wen, J. Pei, C. Yan and J. Huang, *Angew. Chem., Int. Ed.*, 2025, e202503616.
36 Y. Lee, *Solid State Ionics*, 2001, **138**, 273–276.
37 X. Yu, Z. J. Hoffman, J. Lee, C. Fang, L. A. Gido, V. Patel, H. B. Eitouni, R. Wang and N. P. Balsara, *ACS Energy Lett.*, 2022, **7**, 3791–3797.
38 C. Fang, X. Yu, S. Chakraborty, N. P. Balsara and R. Wang, *ACS Macro Lett.*, 2023, **12**, 612–618.
39 C. Fang, S. Chakraborty, Y. Li, J. Lee, N. P. Balsara and R. Wang, *ACS Macro Lett.*, 2023, **12**, 1244–1250.
40 B. D. Mather, K. Viswanathan, K. M. Miller and T. E. Long, *Prog. Polym. Sci.*, 2006, **31**, 487–531.
41 P. Chen, S. Liu, H. Zhou, S. Yan, D. Zhang, X. Pang, X. Chen and X. Wang, *J. Am. Chem. Soc.*, 2025, **147**, 7624–7633.
42 M. Kerner, N. Plylahan, J. Scheers and P. Johansson, *RSC Adv.*, 2016, **6**, 23327–23334.
43 K. Pielichowski and K. Flejtuch, *J. Anal. Appl. Pyrolysis*, 2005, **73**, 131–138.
44 Y. Weng, C.-B. Hong, Y. Zhang and H. Liu, *Green Chem.*, 2024, **26**, 571–592.
45 K. M. Diederichsen, H. G. Buss and B. D. McCloskey, *Macromolecules*, 2017, **50**, 3831–3840.
46 A. Thiam, C. Martinez-Cisneros, Y. Molméret, C. Iojoiu and J.-Y. Sanchez, *Electrochim. Acta*, 2019, **302**, 338–343.
47 K. M. Diederichsen, E. J. McShane and B. D. McCloskey, *ACS Energy Lett.*, 2017, **2**, 2563–2575.
48 D. A. Gribble, L. Frenck, D. B. Shah, J. A. Maslyn, W. S. Loo, K. I. S. Mongcopa, D. M. Pesko and N. P. Balsara, *J. Electrochem. Soc.*, 2019, **166**, A3228–A3234.
49 A. Tron, A. Orue, P. López-Aranguren and A. Beutl, *J. Electrochem. Soc.*, 2023, **170**, 100525.
50 Z. J. Hoffman, A. S. Ho, S. Chakraborty and N. P. Balsara, *J. Electrochem. Soc.*, 2022, **169**, 043502.

51 J. Lee, Z. J. Hoffman, S. Chakraborty, V. Patel and N. P. Balsara, *ACS Energy Lett.*, 2025, **10**, 831–836.
52 Z. Fan, J. Zhang, L. Wu, H. Yu, J. Li, K. Li and Q. Zhao, *Chem. Sci.*, 2024, **15**, 17161–17172.
53 Q. Zhou, M. He, S. Gao, W. Hou, Y. Ma, H. Huo, C. Du, G. Yin and P. Zuo, *Adv. Sci.*, 2025, **12**, 2417169.
54 L. Aguilera, S. Xiong, J. Scheers and A. Matic, *J. Mol. Liq.*, 2015, **210**, 238–242.
55 L. H. B. Nguyen, T. Picard, C. Iojoiu, F. Alloin, N. Sergent, M.-L. Doublet and J.-S. Filhol, *Phys. Chem. Chem. Phys.*, 2022, **24**, 21601–21611.
56 T. D. Pham, A. Bin Faheem and K. Lee, *Small*, 2021, **17**, 2103375.
57 N. Shida, Y. Imada, Y. Okada and K. Chiba, *Eur. J. Org Chem.*, 2020, **2020**, 570–574.
58 M. Wetjen, G.-T. Kim, M. Joost, M. Winter and S. Passerini, *Electrochim. Acta*, 2013, **87**, 779–787.
59 T. H. Wan, M. Saccoccio, C. Chen and F. Ciucci, *Electrochim. Acta*, 2015, **184**, 483–499.
60 N. Rospars, M. Srout, C. Fu, G. Mourouga, M. Mensi and A. Ingenito, *Commun. Mater.*, 2024, **5**, 179.
61 B. D. Adams, J. Zheng, X. Ren, W. Xu and J. Zhang, *Adv. Energy Mater.*, 2018, **8**, 1702097.
62 P. Müller, C. Szczuka, C.-L. Tsai, S. Schöner, A. Windmüller, S. Yu, D. Steinle, H. Tempel, D. Bresser, H. Kungl and R.-A. Eichel, *ACS Appl. Mater. Interfaces*, 2024, **16**, 32209–32219.
63 R. Sahore, A. Mayer, D. Steinle, M. J. Counihan, X. C. Chen, S. Tepavcevic, D. Bresser and A. S. Westover, *J. Electrochem. Soc.*, 2024, **171**, 050505.
64 M. Ebadi, C. Marchiori, J. Mindemark, D. Brandell and C. M. Araujo, *J. Mater. Chem. A*, 2019, **7**, 8394–8404.
65 G. Beamson and D. Briggs, *High Resolution XPS of Organic Polymers: The Scienta ESCA300 Database*, Wiley, Chichester, 1992.
66 M. C. Biesinger, *Appl. Surf. Sci.*, 2022, **597**, 153681.
67 E. K. W. Andersson, C. Sångeland, E. Berggren, F. O. L. Johansson, D. Kühn, A. Lindblad, J. Mindemark and M. Hahlin, *J. Mater. Chem. A*, 2021, **9**, 22462–22471.
68 W. Yu, Z. Yu, Y. Cui and Z. Bao, *ACS Energy Lett.*, 2022, **7**, 3270–3275.
69 T. Weintraut, A. Weiss, S. L. Benz, B. Aktekin, J. Sann and A. Henss, *Adv. Mater. Interfaces*, 2025, **12**, e00392.
70 J. Ko and Y. S. Yoon, *Ceram. Int.*, 2019, **45**, 30–49.
71 H. Xu, Q. Zhu, Y. Zhao, Z. Du, B. Li and S. Yang, *Adv. Mater.*, 2023, **35**, 2212111.
72 A. Lassagne, E. Beaudoin, A. Ferrand, T. N. T. Phan, P. Davidson, C. Iojoiu and R. Bouchet, *Electrochim. Acta*, 2017, **238**, 21–29.
73 D. Devaux, D. Glé, T. N. T. Phan, D. Gigmes, E. Giroud, M. Deschamps, R. Denoyel and R. Bouchet, *Chem. Mater.*, 2015, **27**, 4682–4692.
74 K. Leslie, J. Harlow, D. Rathore, K. Tuul and M. Metzger, *J. Electrochem. Soc.*, 2024, **171**, 040520.
75 Z. Zhang, J. Wang, S. Zhang, H. Ying, Z. Zhuang, F. Ma, P. Huang, T. Yang, G. Han and W.-Q. Han, *Energy Storage Mater.*, 2021, **43**, 229–237.
76 J. □qvist, *J. Phys. Chem.*, 1990, 94, 8021–8024–.
77 J. N. Canongia Lopes, J. Deschamps and A. A. H. Pádua, *J. Phys. Chem. B*, 2004, 108, 2038–2047–.
78 P. G. Bruce and C. A. Vincent, *J. Electroanal. Chem. Interfacial Electrochem.*, 1987, 225, 1–17–.
79 M. Watanabe, S. Nagano, K. Sanui and N. Ogata, *Solid State Ionics*, 1988, 28–30, 911–917–.
80 A. Maradesa, B. Py, T. H. Wan, M. B. Effat and F. Ciucci, *J. Electrochem. Soc.*, 2023, 170, 030502.

